Printed ISSN 1330–0016
Online ISSN 1333–9133
CD ISSN 1333–8390
CODEN FIZBE7

PION STRUCTURE IN QCD: FROM THEORY TO LATTICE TO EXPERIMENTAL DATA

A. P. BAKULEV[a], S. V. MIKHAILOV[a], A. V. PIMIKOV[a] and N. G. STEFANIS[b]

[a]*Bogoliubov Lab. of Theoretical Physics, JINR, 141980 Dubna, Russia*
E-mail addresses: bakulev@theor.jinr.ru, mikhs@theor.jinr.ru, pimikov@theor.jinr.ru

[b]*ITP-II, Ruhr-Universität Bochum, D-44780 Bochum, Germany*
E-mail address: stefanis@tp2.ruhr-uni-bochum.de

Received 13 October 2007; Accepted 20 February 2008
Online 20 June 2008

We describe the present status of the pion distribution amplitude (DA) as it originates from several sources: (i) a nonperturbative approach based on QCD sum rules with nonlocal condensates, (ii) an $O(\alpha_s)$ QCD analysis of the CLEO data on $F^{\gamma\gamma^*\pi}(Q^2)$ with asymptotic and renormalon models for higher twists and (iii) recent high-precision lattice QCD calculations of the second moment of the pion DA. We show predictions for the pion electromagnetic form factor, obtained in analytic QCD perturbation theory, and compare it with the JLab data on $F_\pi(Q^2)$. We also discuss in this context an improved model for nonlocal condensates in QCD and show its consequences for the pion DA and the $\gamma\gamma^* \to \pi$ transition form factor. We include a brief analysis of meson-induced massive lepton (muon) Drell–Yan production for the process $\pi^- N \to \mu^+\mu^- X$, considering both an unpolarized nucleon target and longitudinally polarized protons.

PACS numbers: 11.10.Hi, 12.38.Bx, 12.38.Lg, 13.40.Gp UDC 539.125
Keywords: pion distribution amplitude, electromagnetic form factors, QCD sum rules, factorization, renormalization group evolution, lattice QCD, Drell–Yan production

1. *Introduction*

The pion distribution amplitude (DA) parameterizes the matrix element of the nonlocal axial current on the light cone [1]

$$\langle 0 \,|\, \bar{d}(z)\gamma_\mu\gamma_5\mathcal{C}(z,0)u(0)\,|\,\pi(P)\rangle\Big|_{z^2=0} = \mathrm{i}f_\pi P_\mu \int_0^1 \mathrm{d}x\; e^{\mathrm{i}x(zP)}\varphi_\pi^{\mathrm{Tw-2}}(x,\mu^2)\,. \tag{1}$$

The gauge-invariance of this DA is ensured by the Fock–Schwinger connector [2] (Wilson line)

$$\mathcal{C}(z,0) = \mathcal{P}\exp\left[\mathrm{i}g\int_0^z A_\mu(\tau)\mathrm{d}\tau^\mu\right],$$

inserted between the two quark fields. The physical meaning of this DA is quite evident: it is the amplitude for the transition $\pi(P) \to u(Px) + \bar{d}(P(1-x))$. It is convenient to represent the pion DA using an expansion in terms of Gegenbauer polynomials $C_n^{3/2}(2x-1)$, which are one-loop eigenfunctions of the ERBL kernel [3, 4], i. e.,

$$\varphi_\pi(x;\mu^2) = \varphi^{\mathrm{As}}(x)\left[1 + \sum_{n\geq 1} a_{2n}(\mu^2)\, C_{2n}^{3/2}(2x-1)\right], \tag{2}$$

where $\varphi^{\mathrm{As}}(x) = 6\,x\,(1-x)$ is the asymptotic pion DA. This representation means that all scale dependence in $\varphi_\pi(x;\mu^2)$ is transformed into the scale dependence of the set $\left\{a_2(\mu^2), a_4(\mu^2), \ldots\right\}$. We mention here that the ERBL solution at the 2-loop level is also possible using the same representation [5 − 8].

In order to construct reliable QCD SRs for the pion DA moments, one needs, as has been shown in Refs. [9, 10], to take into account the nonlocality of the QCD vacuum condensates. For an illustration of the nonlocal condensate (NLC) model, we use here the minimal Gaussian model

$$\langle\bar{q}(0)q(z)\rangle = \langle\bar{q}\,q\rangle\, e^{-|z^2|\lambda_q^2/8} \tag{3}$$

with a single scale parameter $\lambda_q^2 = \langle k^2\rangle$ that characterizes the average momentum of quarks in the QCD vacuum. Its value has been estimated in the QCD SR approach and also on the lattice [11 − 14],

$$\lambda_q^2 = 0.35 - 0.55\ \mathrm{GeV}^2. \tag{4}$$

Let us write down, as an example, the NLC QCD SR for the pion DA $\varphi_\pi(x)$. To derive it, one starts from a correlator of the currents $J_{\mu 5}(x) = \bar{d}(x)\,\gamma_\mu\gamma_5\,u(x)$ and $J^\dagger_{\nu 5;N}(0) = \bar{u}(0)\,\gamma_\nu\gamma_5\,(n\nabla)^N d(0)$ with a light-like vector n, $n^2 = 0$ to obtain next SRs for the moments $\langle x^N\rangle_\pi$, and finally to apply the inverse Mellin transform and arrive at $\langle x^N\rangle_\pi \Rightarrow \varphi_\pi(x)$. As a result, we then find

$$f_\pi^2\,\varphi_\pi(x) = \int_0^{s_0}\rho^{\mathrm{pert}}(x;s)\,e^{-s/M^2}\mathrm{d}s + \frac{\alpha_s\langle GG\rangle}{24\pi M^2}\,\varphi_{GG}(x;\Delta) + \frac{8\pi\alpha_s\langle\bar{q}q\rangle^2}{81M^4}\sum_{i=2V,3L,4Q}\varphi_i(x;\Delta) \tag{5}$$

with $\Delta \equiv \lambda_q^2/M^2$ and $\varphi_{GG,2V,3L,4Q}(x;\Delta)$ being contributions of gluon-gluon, quark-antiquark, quark-gluon-antiquark and 4-quark condensates, respectively (see for details Ref. [15]). The local limit $\Delta \to 0$ of this SR is specified by the appearance of δ-functions concentrated at the end-points $x = 0$ and $x = 1$, for example, $\varphi_{4Q}(x; \Delta) = 9[\delta(x) + \delta(1 - x)]$.

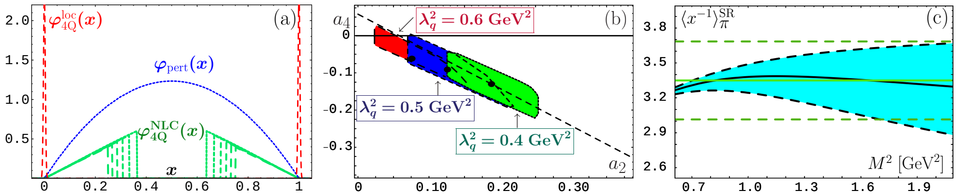

Fig. 1. (a): The contributions to Eq. (5) are shown due to the perturbative loop (dotted line) and the four-quark condensate: $\varphi_{4\mathrm{Q}}^{\mathrm{loc}}(x)$ (standard QCD SRs); $\varphi_{4\mathrm{Q}}^{\mathrm{NLC}}(x, M^2 = 0.55 - 0.80\ \mathrm{GeV}^2)$ (the NLC QCD SRs). Panel (b): Allowed values of the parameters a_2 and a_4 of the bunches (6), evaluated at $\mu^2 = 1.35\ \mathrm{GeV}^2$, for three values of the nonlocality parameter: $\lambda_q^2 = 0.4\,, 0.5,$ and $0.6\ \mathrm{GeV}^2$. Panel (c): The inverse moment $\langle x^{-1} \rangle_\pi$, obtained using the NLC SR (5), is shown as a solid line (central value) with error-bars represented by the dashed lines.

The minimal Gaussian model (3) generates the contribution $\varphi_{4\mathrm{Q}}(x; \Delta)$, shown on the right panel of Fig. 1 in comparison with the perturbative one for the standard (local) and the NLC types of that SR. We see that, due to the completely different behavior of the perturbative and condensate terms in the local QCD SR, it is difficult to reach a reasonable consistency. In contrast, the NLC contribution behaves similarly to the perturbative one. Just for this reason, we have a very good stability in the NLC SR case. After processing SR (5) for the moments $\langle \xi^N \rangle_\pi = \int_0^1 \varphi_\pi(x)\ (2x - 1)^N\, \mathrm{d}x$, we can restore the pion DA $\varphi_\pi(x)$ by demanding that it should reproduce the first five moments $\langle \xi^i \rangle_\pi$, $i = 2\,, 4\,, \ldots, 10$, using to this purpose the minimally possible number of Gegenbauer harmonics in representation (2). It comes out that the NLC SRs for the pion DA yield a bunch of self-consistent two-parameter models at $\mu_0^2 \simeq 1.35\ \mathrm{GeV}^2$,

$$\varphi_\pi^{\mathrm{NLC}}(x; \mu_0^2) = \varphi^{\mathrm{As}}(x) \left[1 + a_2(\mu_0^2)\, C_2^{3/2}(2x - 1) + a_4(\mu_0^2)\, C_4^{3/2}(2x - 1)\right]. \tag{6}$$

The central point corresponds to $a_2^{\mathrm{BMS}} = +0.188$, $a_4^{\mathrm{BMS}} = -0.130$ for $\lambda_q^2 = 0.4$ GeV^2, whereas other allowed values of the parameters a_2 and a_4 are shown on the central panel of Fig. 1 as a slanted rectangle [15]. Because the inverse moments of all these pion DAs equal

$$\langle x^{-1} \rangle_\pi^{\mathrm{bunch}} = 3.17 \pm 0.20\,, \tag{7}$$

being in good agreement with the estimation dictated by an independent SR for this moment, we term this bunch self-consistent. This SR can be obtained through the basic SR (5) by integrating over x and using the weight x^{-1} (at $\mu_0^2 \simeq 1.35$ GeV^2) to find

$$\langle x^{-1}\rangle_\pi^{\rm SR} = 3.30 \pm 0.30\,, \tag{8}$$

shown graphically on the panel (c) of Fig. 1.

It is worth emphasizing that the moment $\langle x^{-1}\rangle_\pi^{\rm SR}$ could be determined only with NLC SRs by virtue of the absence of end-point singularities. Comparison of the obtained pion DA with the Chernyak–Zhitnitsky (CZ) one [16] reveals that, although both DAs are two-humped, they have distinct characteristics: the BMS DA is strongly end-point suppressed, as illustrated in Fig. 2a, while the CZ one is end-point dominated. To display this property more explicitly, we show on panel (b) of this figure the comparison of the BMS and the CZ contributions to the inverse moment $\langle x^{-1}\rangle_\pi$, grouped in different bins and calculated as $\int_x^{x+0.02} u^{-1}\varphi(u)\,{\rm d}u$ (normalized to 100%).

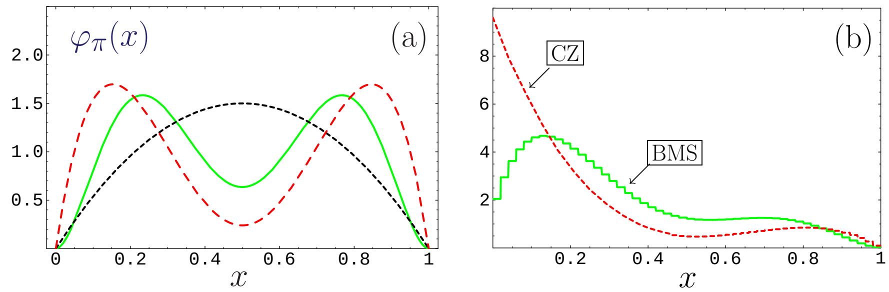

Fig. 2. Panel (a): Comparison of the profiles of three pion DAs: BMS (solid line), CZ (dashed line), and the asymptotic DA (dotted line). Panel (b): Histograms for the contributions of different bins to the inverse moment $\langle x^{-1}\rangle_\pi$ shown for the CZ and the BMS DAs.

2. Analysis of the CLEO data on $F_{\gamma\gamma^*\pi}(Q^2)$

Many studies [17−20, 14, 21] have been performed in the literature to determine the pion DA using the high-precision CLEO data [22] on the pion-photon transition form factor $F_{\pi\gamma^*\gamma}(Q^2)$. In particular, in Ref. [21], we have used light-cone sum rules (LCSR) [17, 18] to the next-to-leading-order accuracy of QCD perturbation theory to examine the theoretical uncertainties involved in the CLEO-data analysis in order to extract more reliably the first two non-trivial Gegenbauer coefficients a_2 and a_4, which parameterize the deviation from the asymptotic expression $\varphi_\pi^{\rm As}$.

Let us clarify why it is advantageous to use LCSRs in analyzing the experimental data on $\gamma^*(Q)\gamma(q) \to \pi^0$ transition form factor. For $Q^2 \gg m_\rho^2$ and $q^2 \ll m_\rho^2$, QCD factorization is valid only in the leading-twist approximation, so that the higher twists are important [23]. The reason is quite clear: if $q^2 \to 0$, one has to take into account the interaction of a real photon at long distances of the order of $O(1/\sqrt{q^2})$. Then, in order to account for the long-distance effects in perturbative QCD, one has to introduce the light-cone DA of the real photon. Instead of doing so, Khodjamirian [17] suggested to use the LCSR approach, which effectively accounts for the long-distances effects of the real photon using quark-hadron duality in the vector channel and a dispersion relation in q^2. Schmedding and Yakovlev used this approach in analyzing the CLEO data on the $\gamma^*\gamma \to \pi$ transition form factor at the level of the next-to-leading-order (NLO) accuracy of the perturbative QCD part of the LCSR [18].

We improved in Refs. [21, 24] the NLO analysis of the CLEO data by taking into account the following key elements: (i) the NLO evolution for both $\varphi(x, Q^2_{\rm exp})$ and $\alpha_s(Q^2_{\rm exp})$ was generalized to include heavy-quark thresholds more accurately; (ii) a relation between the "nonlocality" scale and the twist-4 magnitude $\delta^2_{\rm Tw-4} \approx \lambda_q^2/2$ was employed to reestimate $\delta^2_{\rm Tw-4} = 0.19 \pm 0.02$ at $\lambda_q^2 = 0.4$ GeV^2; (iii) the possibility to extract constraints on $\langle x^{-1}\rangle_\pi$ from the CLEO data and compare them with those we derived before from NLC QCD SRs [15] was exploited.

The results of our analysis in Ref. [21] are displayed in Fig. 3. Solid lines in all figures enclose the 2σ-contours, whereas the 1σ-contours are shown by the dashed lines. The three slanted and shaded rectangles represent the constraints on $(a_2,\ a_4)$ posed by the QCD SRs [15] for different values of $\lambda_q^2 = 0.6,\ 0.5,\ 0.4$ GeV^2 (from the left to the right). All values are evaluated at $\mu^2 = 2.4$ GeV^2 after NLO evolution.

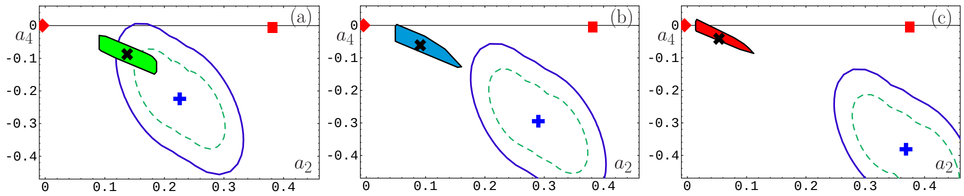

Fig. 3. Three 2σ- and 1σ-contours (solid and dashed lines, correspondingly) of the admissible regions following from the analysis of the CLEO data for different values of λ_q^2: (a) $\lambda_q^2 = 0.4$ GeV^2; (b) $\lambda_q^2 = 0.5$ GeV^2; (c) $\lambda_q^2 = 0.6$ GeV^2.

We see that the CLEO data favor the value of the QCD nonlocality parameter $\lambda_q^2 = 0.4$ GeV^2. We also see from Fig. 3c (and this conclusion was confirmed even with a 20% uncertainty of the twist-four magnitude—cf. Fig. 4a) that the CZ DA (■) is excluded at least at the 4σ-level, whereas the asymptotic DA (◆) is off at the 3σ-level. At the same time, the BMS DA (✖), and most of the bunch (the slanted green-shaded rectangle around the symbol ✖), are inside the 1σ-domain. The instanton-based Bochum (☆) and Dubna (▲) models are near but just outside the 3σ-boundary and only the Krakow model [26], denoted in Fig. 4a by the symbol ✥, is close to the 2σ-boundary.

In Fig. 4a we demonstrate the 1σ-, 2σ- and 3σ-contours (solid, dotted, and dashed contours around the best-fit point (✚)), which have been obtained for values of the twist-4 scale parameter $\delta^2_{\rm Tw-4} = [0.15 - 0.23]$ GeV^2. As one sees from the blue dashed line within the hatched band (corresponding in this figure to the mean value of $\langle x^{-1}\rangle^{\rm SR}_{\pi}/3-1$ and its error bars), the nonlocal QCD sum-rules result with its error bars appears to be in good agreement with the CLEO-constraints on $\langle x^{-1}\rangle^{\rm exp}_{\pi}$ at the 1σ-level. Moreover, the estimate $\langle x^{-1}\rangle^{\rm SR}_{\pi}$ is close to $\langle x^{-1}\rangle^{\rm EM}_{\pi}/3-1 = 0.24\pm 0.16$, obtained in the data analysis of the pion electromagnetic form factor within the framework of a different LCSR method in Ref. [27, 28]. These three independent estimates are in good agreement to each other, giving firm support that the CLEO-data processing, on the one hand, and the theoretical calculations, on the other, are mutually consistent.

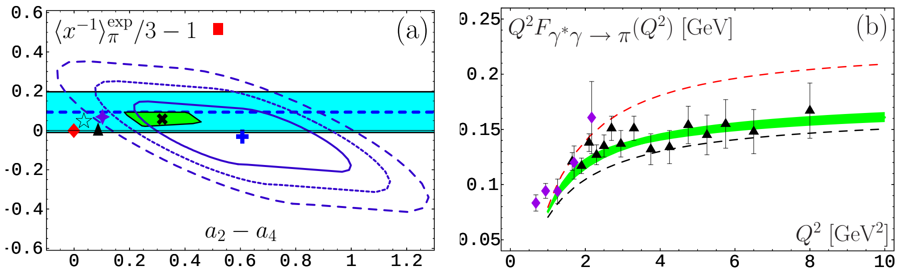

Fig. 4. (a): The results of the CLEO-data analysis for the pion DA parameters ($\langle x^{-1}\rangle^{\rm exp}_{\pi}/3-1$, evaluated at $\mu_0^2 \approx 1$ GeV^2. (b): LCSR predictions for $Q^2 F_{\gamma^*\gamma\to\pi}(Q^2)$ for the CZ DA (upper dashed line), BMS-"bunch" (shaded strip), and the asymptotic DA (lower dashed line) in comparison with the CELLO (diamonds [25]) and the CLEO (triangles [22]) experimental data, evaluated at $\mu^2_{\rm SY} = 5.76$ GeV^2 with the twist-4 parameter value $\delta^2_{\rm Tw-4} = 0.19$ GeV^2 [21].

Another possibility, suggested in Ref. [29], to obtain constraints on the pion DA in the LCSR analysis of the CLEO data, would be to use for the twist-4 contribution, a renormalon-based model, and to relate it to the parameters a_2 and a_4 of the pion DA. Using this method, we obtained in Ref. [24] the renormalon-based constraints for the parameters a_2 and a_4 as shown in Fig. 6? in the form of a 1σ-ellipse (dashed contour).

3. *Dijet E791 data, pion form factor and CEBAF data*

Our findings are further confirmed by the E791 data [30] on diffractive dijet $\pi + A$ production. This is illustrated in Fig. 5a? The main conclusion here is that all considered pion DAs are consistent with these data, with a slight preference for the BMS DA. Indeed, following the convolution procedure of Ref. [31], we found [21] the following values of χ^2 for the three types of pion DAs: 12.56 (asymptotic DA), 10.96 (BMS bunch) and 14.15 (CZ DA).

It is worth mentioning the results of our analysis of the pion electromagnetic form factor using the NLC-based pion DA and analytic perturbative QCD [33]. These results are in excellent agreement with the CEBAF data on the pion form factor, as illustrated in Fig. 5b, where the green strip includes both the NLC QCD SR uncertainties, generated by the bunch of the allowed pion DAs and by the scale-setting ambiguities at the NLO level of QCD perturbation theory.

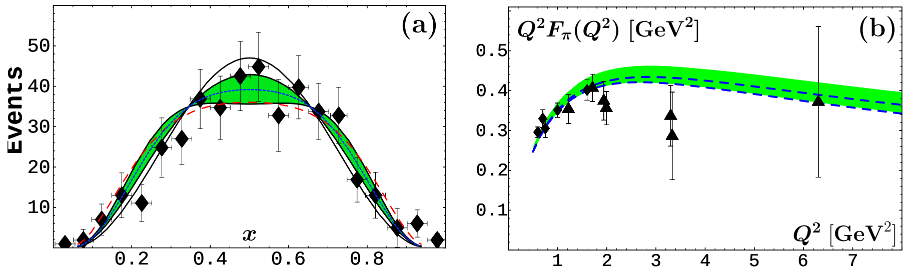

Fig. 5. (a): Comparison with the E791 data on the diffractive dijet production of the BMS "bunch" (shaded strip), the asymptotic DA (solid line), and the CZ (dashed line) model, using the convolution approach of Ref. [31]. (b): The scaled pion form factor calculated with the BMS bunch (shaded strip) and the asymptotic DA (dashed lines) including nonperturbative uncertainties from NLC QCD SRs [15, 32] and the renormalization scheme and scale ambiguity at the $O(\alpha_s^2)$ level [33]. The experimental data are taken from Ref. [34] (diamonds) and Ref. [35] (triangles).

From the phenomenological point of view, the most interesting result here is that the BMS pion DA [15] (out of the "bunch" of similar doubly-peaked endpoint-suppressed pion DAs) yields predictions for the electromagnetic form factor of the pion, which are very close to those obtained with the asymptotic pion DA. Conversely, we see from Fig. 5b that a small deviation of the prediction for the pion form factor from that obtained with the asymptotic pion DA (dashed lines) does not necessarily imply that the underlying pion DA has to be close to the asymptotic profile. Much more important is the behavior of the pion DA in the endpoint region $x \to 0\,, 1$. For more details, we refer to Ref. [33].

4. *New lattice data and pion DA*

Rather recently, new high-precision lattice measurements of the second moment of the pion DA $\langle\xi^2\rangle_\pi = \int_0^1 (2x-1)^2\varphi_\pi(x)\,dx$ appeared [36, 37]. Both cited groups extracted from their respective simulations values of a_2 at the Schmedding–Yakovlev scale $\mu^2_{\rm SY}$ around 0.24, but with different error bars.

It is remarkable that these lattice results are in striking agreement with the estimates of a_2 from both the NLC QCD SRs [15] and also from the CLEO-data analyses, based on LCSR, [18, 21], as illustrated in Fig. 6a, where the lattice results of Ref. [37] are shown in the form of a vertical strip, containing the central value with associated errors. Remarkably, the value of a_2 of the displayed lattice measurements (middle line of the strip) is very close to the CLEO best fit of Ref. [21] (✚).

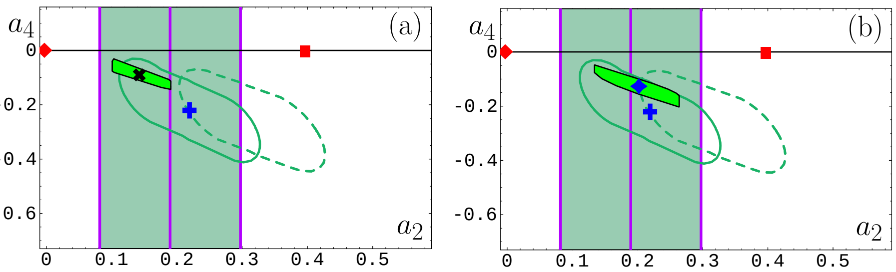

Fig. 6. The results of the CLEO-data analysis for the pion DA parameters a_2 and a_4, evaluated at $\mu^2_{\rm SY} = 5.76$ GeV^2. The lattice results of Ref. [37] are displayed as a shaded area, whereas the renormalon-based 1σ-ellipse of Ref. [24] is denoted by the green dashed line. The small slanted rectangle on panel (a) represents the corresponding results for the BMS-"bunch", whereas the modified, somewhat larger, slanted rectangle corresponding to the improved Gaussian model of QCD vacuum, is shown on panel (b).

5. *Improved model for NLCs and pion DA*

The quark-gluon-antiquark condensates are usually parameterized in the following form

$$
\begin{aligned}
\langle \bar{q}(0)\gamma_\mu \left(-g\sum_a t^a A^a_\nu(y)\right) q(x)\rangle &= (y_\mu x_\nu - g_{\mu\nu}(yx))\overline{M}_1(x^2,y^2,(y-x)^2) \\
&+ (y_\mu y_\nu - g_{\mu\nu}y^2)\overline{M}_2(x^2,y^2,(y-x)^2)\,, \\
\langle \bar{q}(0)\gamma_5\gamma_\mu \left(-g\sum_a t^a A^a_\nu(y)\right) q(x)\rangle &= i\varepsilon_{\mu\nu yx}\overline{M}_3(x^2,y^2,(y-x)^2)\,,
\end{aligned}
$$

where

$$\overline{M}_i(x^2,y^2,z^2) = A_i \iiint\limits_0^\infty {\rm d}\alpha\,{\rm d}\beta\,{\rm d}\gamma\, f_i(\alpha,\beta,\gamma)\, e^{\left(\alpha x^2+\beta y^2+\gamma z^2\right)/4}\,,$$

with $A_{1,2,3} = A_0\left(-\frac{3}{2}, 2, \frac{3}{2}\right)$. The minimal model of the nonlocal QCD vacuum suggests the following Ansatz

$$f_i^{\rm min}\left(\alpha,\beta,\gamma\right) = \delta\left(\alpha-\Lambda\right)\,\delta\left(\beta-\Lambda\right)\,\delta\left(\gamma-\Lambda\right)\,, \tag{9}$$

with $\Lambda = \frac{1}{2}\lambda_q^2$, and faces problems with the QCD equations of motion and the gauge invariance of the 2-point correlator of vector currents. In order to fulfil the QCD equations of motion exactly and minimize the non-transversity of the $V-V$

correlator, an improved version of the QCD vacuum model was suggested in Ref. [32] with

$$f_i^{\rm imp}\left(\alpha,\beta,\gamma\right) = \left(1 + X_i\partial_x + Y_i\partial_y + Y_i\partial_z\right)\delta\left(\alpha - x\Lambda\right)\delta\left(\beta - y\Lambda\right)\delta\left(\gamma - z\Lambda\right), \quad (10)$$

where $\Lambda = \frac{1}{2}\lambda_q^2$ and

$$X_1 = +0.082\,;\; X_2 = -1.298\,;\; X_3 = +1.775\,;\; x = 0.788\,; \quad (11a)$$

$$Y_1 = -2.243\,;\; Y_2 = -0.239\,;\; Y_3 = -3.166\,;\; y = z = 0.212\,. \quad (11b)$$

Then, the NLC sum rules (5) give rise to a modified "bunch" of two-parameter pion DA models (6) at $\mu^2 = 1.35$ GeV^2 [32]. The coordinates of the central point ✥ are $a_2 = 0.268$ and $a_4 = -0.186$. These values correspond to $\langle x^{-1}\rangle_\pi^{\rm bunch} = 3.24 \pm 0.20$, which is in agreement with the result provided by an independent sum rule, viz., $\langle x^{-1}\rangle_\pi^{\rm SR} = 3.40 \pm 0.34$. The allowed values of both bunch parameters a_2 and a_4, after NLO-evolution to $\mu^2 = 5.76$ GeV^2, are shown in Fig. 6 in the form of shaded slanted rectangles around the central points ✖ and ✥.

We emphasize in this context that the BMS model [15], shown in Fig. 6a by the symbol ✖, is inside the allowed region extracted from the improved QCD vacuum model. This means that all characteristic features of the original BMS bunch are also valid for the improved bunch. Again, the NLC-based model DAs are end-point suppressed, though they are doubly humped. We see from Fig. 6b that the improved bunch [32] appears to be in somewhat better agreement with the recent lattice results [37], shown in the form of a vertical strip, containing the central value with its associated errors. Remarkably, the value of a_2 of the displayed lattice measurements (middle line of the strip) is very close to the central point of the improved bunch (✥), whereas the whole admissible region (slanted rectangle) [32] is inside the strip[1] and also inside the standard CLEO 1σ-ellipse. Furthermore, we see

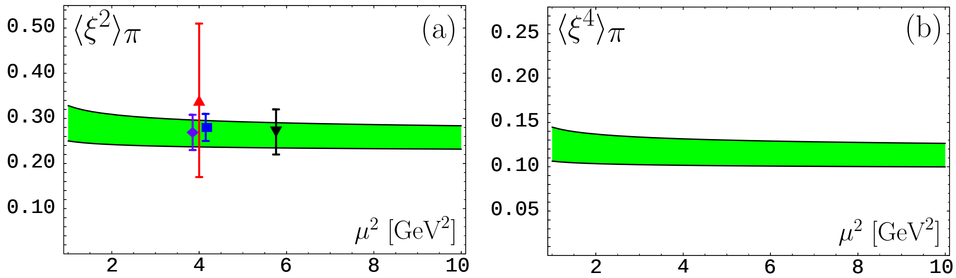

Fig. 7. Evolution of $\langle\xi^2\rangle_\pi(\mu^2)$ (panel (a)) and $\langle\xi^4\rangle_\pi(\mu^2)$ (panel (b)) with $\mu^2 \in 1 - 10$ GeV^2. The green strip on both panels corresponds to the unified results of the QCD Sum Rules with NLCs (minimal and improved models of the QCD vacuum). On the left panel, we also show the lattice results with their corresponding error-bars: ▲ [38], ▼ [36], ◆ [37], ■ [39].

[1]This statement is valid for the BMS "bunch" as well, as can be seen from Fig. 6a.

from this figure and Fig. 7a that the higher the precision of the lattice simulations, the closer they are to the results for $\langle\xi^2\rangle_\pi(\mu^2)$ of the NLC-based QCD SRs. It remains to be seen whether this agreement will persist also for the $\langle\xi^4\rangle_\pi(\mu^2)$ moment shown in Fig. 7b, once its calculation will become possible on the lattice [40].

6. *Pion DA and Drell–Yan πN process*

The DY process is the dominant mechanism to produce lepton pairs with a large invariant mass Q^2 in hadronic collisions, like the $\pi^\pm N$ scattering. In this model, a massive muon pair is created through the electromagnetic annihilation of an antiquark from the beam pion and a quark from the nucleon target, as depicted on the left panel of Fig. 8?.

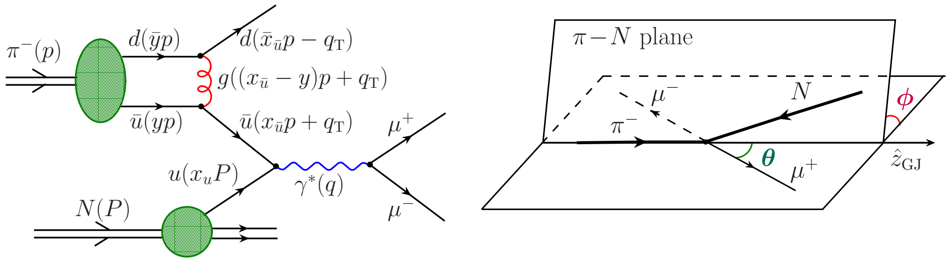

Fig. 8. Left panel: Graphical representation of the Drell–Yan process $\pi^- N \to \mu^+\mu^- X$. Right panel: Angular definitions of the Drell–Yan process in the center of mass frame of the produced massive lepton pair. The axis $\hat{z}_{\mathrm{GJ}}$ denotes the pion direction in the Gottfried–Jackson (GJ) frame.

Here $p_{\bar{u}} = x_{\bar{u}}P$ is the momentum of the annihilating antiquark from the pion. Typical values of the kinematical parameters, $s = (p_\pi + P_N)^2$, $Q^2 = q^2$, and $Q_T^2 = -q_T^2$, see Fig. 8, in the case of the FNAL experiment E615, are: $s = 500\ \mathrm{GeV}^2$, $Q^2 = 16 - 70\ \mathrm{GeV}^2$, and $\rho \equiv Q_T/Q = 0 - 0.5$. As $x_{\bar{u}} \to 1$, $p_{\bar{u}}^2$ becomes large and far spacelike and, therefore, it is sufficient to consider the u-quark to be nearly free and on-shell: $x_u = x_N$ (no transverse momenta). On the right panel of Fig. 8 we show the angular-distribution parameters θ, the polar angle measuring the μ^+ direction in the Gottfried–Jackson system of axes, and ϕ, the azimuthal angle between the $\pi^-\mu^+\mu^-$ and $\pi^- N$ planes in the lepton rest frame.

For the DY reaction with an unpolarized target, the angular distribution of the μ^+ in the pair rest frame can be written in terms of the kinematic variables λ, μ, ν as follows [42],

$$\frac{\mathrm{d}^5\sigma(\pi^- N \to \mu^+\mu^- X)}{\mathrm{d}Q^2\mathrm{d}Q_T^2\mathrm{d}x_L\,\mathrm{d}\cos\theta\mathrm{d}\phi} \propto N(\tilde{x},\rho)\Big(1+\lambda\cos^2\theta+\mu\sin 2\theta\cos\phi+\frac{\nu}{2}\sin^2\theta\cos 2\phi\Big). \quad (12)$$

Adopting this convolution procedure, we found [43] the results presented in Fig. 9: We see that the agreement of the chosen pion DA model with the unpolarized E615

(FNAL) data depends on the value of the parameter ρ. It seems that these data cannot make a clear distinction in favor of one particular pion DA. On the other hand, for the asymmetry of the polarized DY $\pi^- N$ process we found (using the convolution procedure of Ref. [44]) the results displayed in Fig. 10. We may come to the conclusion that the asymmetry $\mathcal{A}(\phi, x_L)$ can be used to discriminate different proposed pion DA models, provided the value of ρ can be fixed by experiment [43].

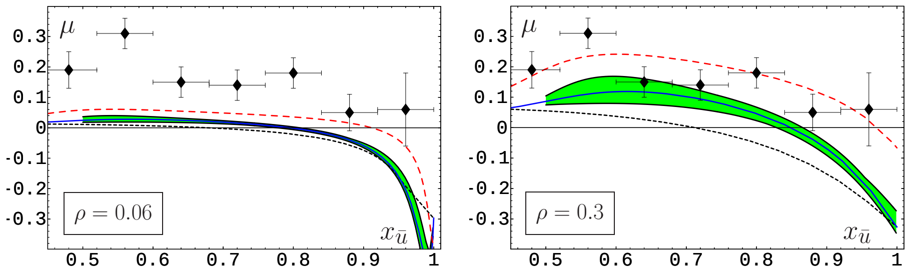

Fig. 9. Results for the angular distribution parameter μ as a function of $x_{\bar{u}} \equiv x_\pi$ for different values of $\rho \equiv Q_T/Q$. The green strip corresponds to the BMS bunch of the pion DAs [15] with the solid line representing the BMS DA, while the dotted solid line shows the result for the asymptotic DA, and the dashed line denotes the prediction for the endpoint-dominated CZ DA. The data are taken from Ref. [41].

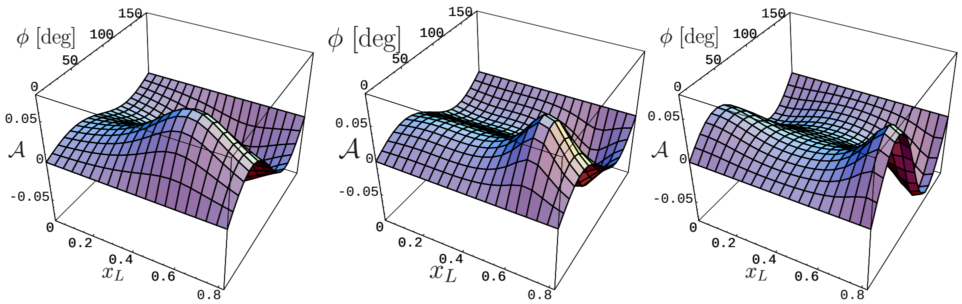

Fig. 10. 3D-plots of the azimuthal asymmetry $\mathcal{A}(\phi, x_L, \rho = 0.3)$ at $q^2 = 16$ GeV^2 and $s = 100$ GeV^2 for three different choices of the pion DA: Asymptotic (left), BMS model (center) and CZ model (right).

7. *Conclusions*

Let us conclude with the following observations:
(i) The NLC QCD SR method for the pion DA gives us admissible bunches of pion DAs for each value of $\lambda_q^2 \gtrsim 0.4$ GeV^2. (ii) The NLO LCSR method produces new constraints on the pion DA parameters (a_2 and a_4) in conjunction with the

CLEO data. (iii) Comparing the results of the NLC SRs with the new CLEO-data constraints, allows us to fix the value of the QCD vacuum nonlocality to be $\lambda_q^2 \simeq 0.4$ GeV^2. (iv) The bunch of pion DAs from NLC QCD SRs agrees well with the E791-data on the diffractive dijet $\pi + A$ production, with the JLab F(pi) data on the pion electromagnetic form factor, and with the latest high-precision lattice data. (v) Taking into account the QCD equations of motion for the NLCs and the transversity of the vacuum polarization, one can shift the pion DA bunch just inside the 1σ-ellipse of the CLEO-data constraints. (vi) In the polarized Drell–Yan $\pi^- N$ process one might be able to discriminate among different pion DAs, once the value of ρ will be known from measurements.

Acknowledgements

One of us (A. P. B.) would like to thank the organizers of the Conference "Hadron Structure–07" (Modra-Harmónia, Slovakia, Sept. 3–7, 2007) for the invitation and support. This work was supported in part by the Russian Foundation for Fundamental Research, grants No. 06-02-16215 and 07-02-91557, the BRFBR–JINR Cooperation Programme (contract No. F06D-002), the Heisenberg–Landau Programme under grant 2007 and the Deutsche Forschungsgemeinschaft (project DFG 436 RUS 113/881/0).

References

[1] A. V. Radyushkin, Dubna preprint P2-10717 (1977) [hep-ph/0410276].

[2] N. G. Stefanis, Nuovo Cim. A **83** (1984) 205.

[3] A. V. Efremov and A. V. Radyushkin, Phys. Lett. B **94** (1980) 245; Teor. Mat. Fiz. **42** (1980) 147 [Theor. Math. Phys. **42** (1980) 97].

[4] G. P. Lepage and S. J. Brodsky, Phys. Lett. B **87** (1979) 359; Phys. Rev. D **22** (1980) 2157.

[5] S. V. Mikhailov and A. V. Radyushkin, Nucl. Phys. B **273** (1986) 297.

[6] E. P. Kadantseva, S. V. Mikhailov and A. V. Radyushkin, Sov. J. Nucl. Phys. **44** (1986) 326.

[7] D. Müller, Phys. Rev. D **49** (1994) 2525; ibid. D **51** (1995) 3855.

[8] A. P. Bakulev and N. G. Stefanis, Nucl. Phys. B **721** (2005) 50.

[9] S. V. Mikhailov and A. V. Radyushkin, JETP Lett. **43** (1986) 712; Sov. J. Nucl. Phys. **49** (1989) 494; Phys. Rev. D **45** (1992) 1754.

[10] A. P. Bakulev and S. V. Mikhailov, Phys. Lett. B **436** (1998) 351.

[11] V. M. Belyaev and B. L. Ioffe, ZhETF **83** (1982) 876.

[12] A. A. Ovchinnikov and A. A. Pivovarov, Sov. J. Nucl. Phys. **48** (1988) 721.

[13] M. D'Elia, A. Di Giacomo and E. Meggiolaro, Phys. Rev. D **59** (1999) 054503.

[14] A. P. Bakulev and S. V. Mikhailov, Phys. Rev. D **65** (2002) 114511.

[15] A. P. Bakulev, S. V. Mikhailov and N. G. Stefanis, Phys. Lett. B **508** (2001) 279; in *Proc. 36th Rencontres De Moriond QCD and Hadronic Interactions*, 17–24 Mar 2001, Les Arcs, France, edited by J. T. T. Van World Scientific, Singapore (2002), pp. 133.

[16] V. L. Chernyak and A. R. Zhitnitsky, Nucl. Phys. B **201** (1982) 492; ibid., B **214** (1983) 54(E).

[17] A. Khodjamirian, Eur. Phys. J. C **6** (1999) 477.

[18] A. Schmedding and O. Yakovlev, Phys. Rev. D **62** (2000) 116002.

[19] N. G. Stefanis, W. Schroers and H.-C. Kim, Phys. Lett. B **449** (1999) 299; Eur. Phys. J. C **18** (2000) 137.

[20] E. Ruiz Arriola and W. Broniowski, Phys. Rev. D **66** (2002) 094016.

[21] A. P. Bakulev, S. V. Mikhailov and N. G. Stefanis, Phys. Rev. D **67** (2003) 074012; Phys. Lett. B **578** (2004) 91.

[22] J. Gronberg *et al.*, Phys. Rev. D **57** (1998) 33.

[23] A. V. Radyushkin and R. Ruskov, Nucl. Phys. B **481** (1996) 625.

[24] A. P. Bakulev, S. V. Mikhailov, and N. G. Stefanis, Phys. Rev. D **73** (2006) 056002.

[25] H. J. Behrend et al., Z. Phys. C **49** (1991) 401.

[26] M. Praszałowicz and A. Rostworowski, Phys. Rev. D **64** (2001) 074003.

[27] V. M. Braun, A. Khodjamirian and M. Maul, Phys. Rev. D **61** (2000) 073004;

[28] J. Bijnens and A. Khodjamirian, Eur. Phys. J. C **26** (2002) 67.

[29] S. S. Agaev, Phys. Rev. D **72** (2005) 114010.

[30] E. M. Aitala et al. (Fermilab E791), Phys. Rev. Lett. **86** (2001) 4768.

[31] V. M. Braun et al., Nucl. Phys. B **638** (2002) 111.

[32] A. P. Bakulev and A. V. Pimikov, Acta Phys. Polon. B **37** (2006) 3627; PEPAN Lett. **4** (2007) 637; Int. J. Mod. Phys. A **22** (2007) 654.

[33] A. P. Bakulev et al., Phys. Rev. D **70** (2004) 033014.

[34] J. Volmer et al., Phys. Rev. Lett. **8** (2001) 1713.

[35] C. N. Brown et al., Phys. Rev. D **8** (1973) 92; C. J. Bebek et al., Phys. Rev. D **13** (1976) 25.

[36] L. Del Debbio, Few Body Syst. **36** (2005) 77.

[37] V. M. Braun et al., Phys. Rev. D **74** (2006) 074501.

[38] G. Martinelli and C. T. Sachrajda, Nucl. Phys. B **306** (1988) 865.

[39] D. Antonio et al., PoS (Lattice 2007) **369** (2007) 1977.

[40] V. Braun and D. Müller, arXiv:0709.1348 [hep-ph].

[41] J. S. Conway et al., Phys. Rev. D **39** (1989) 92.

[42] A. Brandenburg et al., Phys. Rev. Lett. **73** (1994) 939.

[43] A. P. Bakulev, N. G. Stefanis and O. V. Teryaev, Phys. Rev. D **76** (2007) 074032; arXiv:0706.4222 [hep-ph].

[44] A. Brandenburg, D. Müller and O. V. Teryaev, Phys. Rev. D **53** (1996) 6180.

STRUKTURA PIONA U QCD: OD TEORIJE DO REŠETKE I EKSPERIMENTALNIH PODATAKA

Opisujemo sadašnje poznavanje raspodjelne amplitude piona (DA) kako je određuju tri pristupa: (i) neperturbativni računi na osnovi zbrojnih pravila QCD s nelokalnim kondenzatima, (ii) $O(\alpha_s)$ QCD analiza podataka CLEO reda α_s za $F^{\gamma\gamma^*\pi}(Q^2)$ s asimptotskim i renormalon modelima za više tvistove i (iii) nedavni QCD računi na rešetci visoke točnosti za drugi moment pionske DA. Izlažemo predviđanja za pionski elektromagnetski strukturni faktor, izveden u analitičkoj teoriji smetnje QCD-a, te ga uspoređujemo s podacima iz JLAB-a za $F_\pi(Q^2)$. U okviru toga, raspravljamo i poboljšan model za nelokalne kondenzate QCD-a i pokazujemo njegove učinke na pionsku DA i na prijelazni strukturni faktor $\gamma\gamma^* \to \pi$. Uključujemo i kratku analizu Drell–Yanovog procesa tvorbe teskog leptona (miona) procesom $\pi^- N \to \mu^+\mu^- X$, razmatrajući nepolariziranu nukleonsku metu i longitudinalno polarizirane protone.